Sexual representation of social memory in the ventral CA1 neurons

Authors: Akiyuki Watarai[1]†, Kentaro Tao[1]†, Teruhiro Okuyama[1]*

Affiliations:

[1]Laboratory of Behavioral Neuroscience, Institute for Quantitative Biosciences, The University of Tokyo; Tokyo, 1130032, Japan.

*Corresponding author. Email: okuyama@iqb.u-tokyo.ac.jp

†These authors contributed equally to this work.

Abstract:

Recognizing familiar individuals is crucial for adaptive social interactions among animals. However, the multidimensional nature of social memory encompassing sexual information remains unelucidated. We found that neurons in the ventral CA1 region (vCA1) of the mouse hippocampus encoded the identities and social properties, specifically sex and strain, of familiar conspecifics by using both rate and theta-based temporal coding. Optogenetic reactivation of social memories of females, but not males, induced place preference. Ablation of the upstream medial amygdala (MeA) or the hippocampal dorsal CA2 region (dCA2) disrupted the representation of sex and the sexual dimorphism of social memory valence. Selective reactivation of overlapping neural populations of distinct female social memories representing the female sex was sufficient to induce preference. Thus, vCA1 neurons employ dual coding schemes to represent the identities and social properties of familiar conspecifics as a cohesive memory.

One-Sentence Summary:

Social memory in the mouse ventral hippocampus maps the identities and social properties of familiar conspecifics.

Main Text:

The hippocampus plays a crucial role in the integration of multimodal information into a conceptualized cognitive map, which is fundamental for recalling specific experiences and guiding behaviors (*1*). Social memory is a key component of episodic or declarative memory, which enables the recognition of familiar individuals. Extensive animal studies, particularly using rodent models, have underscored the crucial role of the hippocampus in processing social memory. Located along the hippocampal septotemporal axis, the dorsal CA2 region (dCA2) specializes in encoding social stimuli (*2*, *3*), whereas the ventral CA1 region (vCA1), which receives projections from the dCA2 (*4*), is responsible for storing memories of familiar conspecifics (*5*) through the temporal coordination of neuronal population activities (*6*). Notably, a recent study of rats revealed that neuronal responses in the vCA1 to familiar conspecifics showed greater variability among individual females than the responses among males (*7*), and this suggested a potential sexually dimorphic component in hippocampal social memory. Despite significant advances, the neural mechanisms whereby hippocampal networks assemble various elements of social information, such as genetic and physical traits (including sex), into cohesive social memories, remain largely unelucidated.

Nonlinear mixed representation of familiar conspecifics by vCA1 neurons

To investigate how vCA1 neurons respond to different familiar conspecifics, we developed a behavioral paradigm wherein mice (n = 6 adult C57BL/6 male mice) implanted with a high-density silicon probe in the vCA1 (Fig. 1A) explored the arena and interacted with four different familiarized conspecifics that comprised either a female or a male mouse of the BALB/c or C3H strains (BF, BM, CF, and CM; Fig. 1B and fig. S1). The examination of vCA1 neural activity revealed that putative pyramidal cells (fig. S2A; see Materials and Methods for the criteria) were activated by interaction with a specific mouse stimulus (Fig. 1C and D; additional examples are shown in fig. S2B), and its associated properties, including sex and strain (fig. S2C). To classify neurons according to their response selectivity to social stimuli, we performed a two-way ANOVA test (*8*, *9*) with the main factors being sex/strain and an interaction effect on the neuronal firing rate during social interaction. This generated eight subpopulations with distinct activity patterns against social stimuli (Fig. 1G and fig. S2D). Among the entire population of recorded putative pyramidal cells, 26% (49/187) and 39% (73/187) showed significant main

effects of sex and strain, respectively. Additionally, 26% (49/187) encoded a significant nonlinear interaction between sex and strain (Fig. 1E). Both groups of sex and strain cells, hereafter jointly referred to as social property cells, comprised a statistically comparable number of neurons evincing a preference for either female or male sex, and either the BALB/c or C3H strain (Fig. 1F). The overall firing rates were comparable among the sex, strain, and social identity cells (fig. S2E).

Multiplexed coding of social identity and properties

Based on the neuronal activity during social interactions, we trained a set of linear classifiers (Fig. 1H). All classifiers achieved significantly higher decoding accuracies than the null models, which were constructed by circularly shifting event labels (fig. S3A), both at the group (fig. 1I) and individual subject levels (fig. S3B). The linear combination of classifiers for sex and strain did not incorporate the high decoding accuracy of the identity classifier (Fig. 1J), suggesting that nonlinear social memory information is embedded in vCA1 population activity. Although the social interaction sequences exhibited a nonrandom pattern characterized by consecutive staying and switching events, the classifier constructed using real labels significantly outperformed the surrogate classifier, constructed using labels shifted by only one (Fig. 1K and fig. S3C). Corresponding to the transient rise in the firing rate during social interactions (Fig. 1D), we observed that the decoding accuracy of the identity classifiers increased over time as the subject mice approached the stimulus and poked into the social chamber (Fig. 1L). This was the case for both sex and strain classifiers (fig. S3D). To ascertain whether specific subpopulations of neurons encode social properties, we analyzed the weights assigned to each neuron by using classifiers trained to decode both sex and strain (Fig. 1M and fig. S4A). A significant positive correlation between sex and strain was observed across all recorded pyramidal cells (Fig. 1M), which was also evident in the simultaneously recorded pyramidal cells from four of the six subjects (fig. S4B). These findings suggest that a subset of vCA1 neurons modulates the encoding of mixed social memory information. A comparison of the relative importance based on the single-cell classification (Fig. 1E) revealed that sex cells were more crucial for decoding sex compared to strain cells and non-social cells, which were equally below the average importance; strain cells were more influential than sex cells and non-social cells, both of which showed comparable below average importance (Fig. 1N).

To assess whether the representation of social properties conveyed generalized information across conditions, we trained a linear classifier using pseudo-population data derived from a subset of conditions (e.g., interactions with female mice only) to discriminate a pair of social stimuli (BF and CF) and then tested its decoding accuracy using data from the complementary conditions (BM and CM). Both sex classifiers across strains (fig. S5A), and strain classifiers across sexes (fig. S5E) exhibited significantly higher cross-condition generalization performance (CCGP) (*10*) than their respective null models (figs. S5B and F). The strain classifier trained on the males was less accurate than that trained on the females (fig. S5G), which is in line with a previous study which demonstrated that vCA1 neuronal responses to females exhibited greater diversity among individual females than among males (*7*).

Theta-based temporal coding of social memory information

A detailed analysis of the neuronal firing patterns showed that a social identity cell exhibited phase locking of spike timings with the hippocampal theta trough (Fig. 2A), which corresponded to a transient increase in theta-band spiking activity that was coherent with theta oscillations (Fig. 2B). A comparison of spike-LFP coherence at the onset of social interactions showed that social cells exhibited greater phase locking to the theta rhythm than did non-social cells (Fig. 2C). Social and non-social cells displayed distinct theta phase preferences, with the former favoring the trough and the latter spanning from the ascending phase to near the peak (Fig. 2D and 2E). Cells encoding social identity and properties showed a preference for the theta trough; however, social identity cells exhibited a more pronounced concentration around the trough (Fig. 2F). During interactions with preferred versus non-preferred social stimuli for each cell, only social property cells demonstrated a shift toward earlier theta phases, which was indicative of transient phase precession (Fig. 2G and 2H). Although interactions with preferred stimuli led both cell types to favor the theta trough, in contrast to social identity cells, social property cells uniquely preferred later theta phases when faced with non-preferred stimuli (Fig. 2I).

To further elucidate the temporal coding structure of vCA1 activity during social interactions, we compared the pairwise distances of neuronal activity and the time lags between the spikes of the two corresponding cells at theta timescales (Fig. 2J). Only cell pairs exhibiting significant theta modulation in their spike cross-correlograms (CCGs) were included ($P<0.01$, permutation test; Figs. S6B), with a significantly higher proportion of social cells (365/1304 pairs, 28.0%) than of

nonsocial cells (33/517 pairs, 6.0%) (fig. S6C). Among pairs of social cells, but not nonsocial cells, a significant positive correlation was observed between the activity distance and the temporal peak shift of the smoothed CCGs, which was more pronounced when only pairs of either two sex cells or two strain cells were analyzed (Fig. 2K). Furthermore, we classified pairs of social property cells based on whether the two cells had the same preference for either sex or strain of social stimuli (Fig. 2L). As expected, activity distances between cell pairs with identical social property preferences were significantly shorter than those between pairs with different social property preferences (Fig. 2M). Notably, the temporal shifts in the CCG peaks were shorter for pairs with the same preference than for those with different preferences (Fig. 2N). These results underscore a rate and temporal coding strategy in neurons that represent social identities and properties, with a notable divergence of theta phase precision in social property cells (Fig. 2O).

Reactivation of female social memory induces place preference

To capture the representation of sex in social memory, we utilized recently developed techniques for observation and manipulation of engrams (*11*, *12*). Specifically, we combined activity-dependent cell labeling using a virus-mediated system with immunohistochemical cell labeling for immediate early gene expression. Mice were injected with two adeno-associated viruses (AAVs) into the vCA1: one expressing the tetracycline transcriptional activator (tTA) driven by the *c-fos* promoter (AAV2-c-fos:tTA) and the other expressing histone-GFP regulated by the tetracycline response element (TRE) when doxycycline (dox) was absent from the diet (AAV5-TRE:HTG) (Fig. 3A). This enabled the genetic labeling of the neurons that were activated during the first social interaction. For the second social interaction, we used c-Fos immunostaining to visualize the activated neurons (Fig. 3B). The mice were divided into three groups as follows: mice that interacted first with a female BALB and then a female C3H (FF), mice that interacted with a female BALB and then a male C3H (FM), and mice that interacted with a male BALB and then a male C3H (MM) (Fig. 3C). Although all groups displayed a comparable number of active neurons during both the first (HTG^+) and second ($c\text{-}Fos^+$) interactions, the group that interacted with social stimuli of different sexes (FM) showed a significantly lower number of neurons that were double-labeled with HTG and c-Fos as well as a reduced proportion of double-positive neurons among the HTG^+ neurons (Fig. 3D, 3E). These results suggest that distinct

social memory neurons encode the representation of sex, and this corroborates the results of neural recordings (Fig. 1).

To examine whether the social memory of a conspecific carried a specific valence, we employed an optogenetic conditioned place preference (optoCPP) test (*13*) by injecting AAV9-TRE:ChR2-EYFP or AAV9-TRE:EYFP into the vCA1 of c-fos:tTA mice and implanting optic fibers directly above the injection site (Fig. 3F). When the subject mouse was off-dox for 48 h (Fig. 3G), 2-hour exposure to either a female or male C3H mouse resulted in sparse transgene expression (Fig. 3H). Light stimulation of the social memory engram linked to a female conspecific, but not a male, induced a positive reinforcing effect on post-test (day 5), as well as a real-time place preference during the conditioning phase (days 2−4; Fig. 3I−K). Furthermore, this sexually dimorphic effect on social memory reactivation was observed when female or male BALB mice were used to label the engram (fig. S7), suggesting that the representation of the female sex had a general positive valence, regardless of the strain of the social stimulus.

To determine whether vCA1 neurons are essential for CPP induced by the presence of a female conspecific, we first performed a CPP test using female and male mice positioned opposite each other (Fig. 3L), and confirmed that the female mouse elicited both real-time and conditioned place preferences (Fig. 3M). Next, CA1 pyramidal cell-specific Cre transgenic (Trpc4-Cre) mice (*5*) were injected with AAVs encoding Cre-inducible inhibitory opsin (AAV5-EF1α:DIO-eArch3.0-EYFP) or just a fluorescence protein (AAV5-EF1α:DIO- EYFP) into bilateral vCA1 (Fig. 3N), which led to robust transgene expression (Fig. 3O). Optogenetic inhibition of vCA1 pyramidal neurons during conditioning did not alter either real-time or conditioned place preferences (Fig. 3P and Q), and thereby provided evidence that online neural activity in the vCA1 is not essential for immediate induction or memory formation for place preference.

MeA and dCA2 are essential for sex-specific valence of social memory

Neurons in the medial amygdala (MeA) exhibit sexually dimorphic responses to social stimuli (*14*, *15*) – a characteristic that underpins pathway-specific control of distinct social behaviors (*16*, *17*). To explore the role of the MeA in shaping the representation of sex in social memory, we pharmacologically ablated MeA neurons by injecting AAVs that encoded the Cre-inducible diphtheria toxin receptor (DTR; AAV2-CAG:FLEX-DTR-EGFP) and AAV2-EF1α:mCherry-

IRES-Cre into the bilateral MeA of c-fos:tTA mice (Fig. 4A). Intraperitoneal administration of diphtheria toxin (DT) 5 weeks after the virus injection caused near-complete loss of EGFP-positive neurons in the MeA (Fig. 4B). In line with previous studies (*18*, *19*), mice showed a decreased preference for females and displayed mild deficits in social recognition memory 1 week after ablation (fig. S8). After surgery for MeA ablation, AAV5-TRE:HTG was bilaterally injected into the vCA1 of c-fos:tTA mice similarly as in the above-described dual-labeling experiment (Fig. 4C). In contrast to the results from mice with an intact MeA (Fig. 3E), we observed a similar number of c-Fos^{+}HTG^{+} double-positive neurons and a consistent proportion of double-positive neurons among the HTG^{+} neurons across all three groups (Fig. 4D). To determine whether the MeA was crucial for the sex-specific positive valence of social memory, we conducted an optoCPP test after ablation (Fig. 4E). Despite not suppressing the positive reinforcing effect of stimulating female social memory, MeA neuronal ablation induced conditioned place preference in mice that had been labeled and reactivated the social memory of male mice (Fig. 4F and G). These results suggest that the ablation of MeA disrupted the representation of sex and the sexual dimorphism of social memory valence.

The dorsal CA2 region of the hippocampus (dCA2) plays an essential role in encoding and recalling social memory (*2*, *20*, *21*) through projections to the downstream vCA1 (*4*). To assess the contribution of the dCA2 to the sex-specific positive valence of social memory, we ablated dCA2 neurons and conducted an opto-CPP test (Fig. 4H and J). Two weeks after injecting an AAV encoding Cre-inducible DTR into the dCA2 of double transgenic mice with CA2-specific Map3k15-Cre (*22*) and c-fos:tTA transgenes, intraperitoneal DT administration induced a complete loss of EGFP-positive neurons in the dCA2 (Fig. 4I). Similar to MeA ablation, the ablation of dCA2 neurons induced a conditioned place preference in mice, which was labeled and reactivated the social memory of both female and male mice (Fig. 4K and L).

Intersectional activation of female social memories induces place preference

To ascertain whether the observed place preference is specifically associated with the activation of sexual representation in female social memory and whether such activation alone can elicit a positive reinforcing effect, we employed a two-step intersectional labeling technique. We injected AAVs encoding a TRE-inducible excitatory opsin (AAV9-TRE:DIO-ChR2-tdTomato), along with AAVs for an engineered Cre recombinase (AAV5-c-fos:ER^{T2}CreER^{T2}-PEST) and

tTA (AAV2-c-fos:tTA), both of which were regulated by the *c-fos* promoter, into the bilateral vCA1 of wild-type mice (Fig. 4M). Initial social interactions in the presence of 4-hydroxytamoxifen (4-OHT) enabled *c-fos*-dependent Cre/lox recombination, which formed the basis for later gene expression. Following a 1-week interval, to ensure the resetting of the CreER system, the second social interaction in the absence of Dox triggered *c-fos*-dependent activation of the tTA/TRE system that induced ChR2 expression (Fig. 4N, O and fig. S9). This sequence of manipulations ensured the exclusive expression of ChR2-tdTomato in neurons that were reactivated during both social encounters. The selective reactivation of neuronal populations shared between two female social memories, representing the female sex, leads to the development of place preferences. In contrast, the reactivation of neurons associated with male representation did not produce this effect (Fig. 4P and Q).

Discussion

There has been significant progress in uncovering neural circuits that process sex and individual information in rodents and these range from the vomeronasal system (*23*, *24*) to subcortical brain regions (*15*, *25*) and extending to higher-order cortical areas (*26*, *27*). In the present study, we demonstrated that mouse vCA1 neurons use two complementary encoding schemes to represent familiarized conspecifics. First, a subset of neurons displays nonlinear mixed selective responses (*28*, *29*) to a specific combination of sex and strain of individuals and are called social identity cells, which resemble the concept-like cells in the human and primate hippocampus (*30*, *31*). Second, a separate group of neurons responds specifically to either the sex or strain of individuals, and collectively enable the construction of a low-dimensional, generalized representational map of social properties. The synergistic use of these two encoding strategies potentially facilitates an optimal population code for encoding familiarized conspecifics that are embedded in the social space (*32*) both in terms of robustness and efficiency (*33*, *34*).

The spike timing of hippocampal pyramidal cells undergoes a progressive shift from the ascending phase to the trough of hippocampal theta oscillations – a phenomenon known as phase precession (*35*, *36*), which collectively encodes the temporally compressed spatial sequence of an animal's past, current, and future trajectories (*37*, *38*) as well as the nonspatial sequence of discrete events (*39*) or the passage of time (*40*). Neuronal population activities in the vCA1 are temporally organized by the hippocampal theta rhythm during social interactions (*6*), the specific

relationship between this organization and the representational geometry of social information is unelucidated. In this study, we demonstrated that neurons associated with social identity are predominantly activated around the trough of the theta rhythm that is independent of social stimuli, whereas neurons that represent social properties tend to fire during the ascending phase and shift their preference to an earlier phase during interactions with preferred stimuli. In the dorsal hippocampus, the spike timings of place cells are jointly influenced by two primary upstream afferent inputs at the theta timescale – with one originating from the hippocampal CA3 region and the other from entorhinal cortex layer 3 (EC3) (*41*), wherein a stronger EC3 input leads to a broader range of theta phase precession (*42*) particularly in a perceptual stimuli-enriched environment (*43*). Analogously, the spike timings of social property cells may be more strongly modulated by EC3 inputs than those of social identity cells, and leverage a wider range of hippocampal theta phases to construct a generalized map that represents multiple dimensions of social space.

The optogenetic reactivation of social memories linked to female, but not male, conspecifics exhibited a positive reinforcing effect. In addition, we demonstrated that the intersectional reactivation of two distinct female social memories was sufficient to induce this effect. Consistent with the results of the electrophysiological recordings, these findings suggest that distinct neuronal populations in the vCA1 region represent the sex information of familiar individuals. Furthermore, we demonstrated that ablation of the MeA, a key brain region that is essential for processing sexually dimorphic social sensory signals that emerge from the vomeronasal pathway (*15*, *23*, *24*), disrupted the representation of sex in the vCA1 and transformed the behavioral outcome of the activation of the social memory of male conspecifics into that of female conspecifics. Similarly, the ablation of dCA2, which plays a pivotal role in encoding social memory (*2*, *3*), leads to nondiscriminative place preference by activating vCA1 social memories, irrespective of the sex of the stimuli. The activation of imperfect social memory, which lacks sex-specific information or high-dimensional features of individual conspecifics, could exert a positive reinforcing effect by unmasking the inherently rewarding nature of social information (*44*) or by inducing an internal state akin to social novelty, which can elicit conditioned place preferences (*45*). Although functional connectivity is not fully understood, both the MeA and dCA2 send direct and indirect projections to the vCA1 (*4*, *46*, *47*). These afferents presumably entrain vCA1 social cells at specific theta phases with distinct frequencies, which parallel CA3 and EC3 inputs, similar to place- and odor-encoding cells in the piriform

cortex (*48*). Alternatively, the development of social property cells into social identity cells may represent a maturation process, wherein ultimately, multiple sensory inputs are integrated into a sparse conceptual representation of social identity (*31*, *49*).

References

1. H. Eichenbaum, N. J. Cohen, Can we reconcile the declarative memory and spatial navigation views on hippocampal function? *Neuron* **83**, 764–770 (2014).

2. F. L. Hitti, S. A. Siegelbaum, The hippocampal CA2 region is essential for social memory. *Nature* **508**, 88–92 (2014).

3. A. Oliva, A. Fernández-Ruiz, F. Leroy, S. A. Siegelbaum, Hippocampal CA2 sharp-wave ripples reactivate and promote social memory. *Nature* **587**, 264–269 (2020).

4. T. Meira, F. Leroy, E. W. Buss, A. Oliva, J. Park, S. A. Siegelbaum, A hippocampal circuit linking dorsal CA2 to ventral CA1 critical for social memory dynamics. *Nat. Commun.* **9**, 4163 (2018).

5. T. Okuyama, T. Kitamura, D. S. Roy, S. Itohara, S. Tonegawa, Ventral CA1 neurons store social memory. *Science* **353**, 1536–1541 (2016).

6. K. Tao, M. Chung, A. Watarai, Z. Huang, M.-Y. Wang, T. Okuyama, Disrupted social memory ensembles in the ventral hippocampus underlie social amnesia in autism-associated Shank3 mutant mice. *Mol. Psychiatry* **27**, 2095–2105 (2022).

7. R. P. Rao, M. von Heimendahl, V. Bahr, M. Brecht, Neuronal Responses to Conspecifics in the Ventral CA1. *Cell Rep.* **27**, 3460-3472.e3 (2019).

8. M. Rigotti, O. Barak, M. R. Warden, X.-J. Wang, N. D. Daw, E. K. Miller, S. Fusi, The importance of mixed selectivity in complex cognitive tasks. *Nature* **497**, 585–590 (2013).

9. W. Dang, R. J. Jaffe, X.-L. Qi, C. Constantinidis, Emergence of Nonlinear Mixed Selectivity in Prefrontal Cortex after Training. *J. Neurosci.* **41**, 7420–7434 (2021).

10. S. Bernardi, M. K. Benna, M. Rigotti, J. Munuera, S. Fusi, C. D. Salzman, The Geometry of Abstraction in the Hippocampus and Prefrontal Cortex. *Cell* **183**, 954-967.e21 (2020).

11. S. A. Josselyn, S. Köhler, P. W. Frankland, Finding the engram. *Nat. Rev. Neurosci.* **16**, 521–534 (2015).

12. S. A. Josselyn, S. Tonegawa, Memory engrams: Recalling the past and imagining the future. *Science* **367** (2020).

13. R. L. Redondo, J. Kim, A. L. Arons, S. Ramirez, X. Liu, S. Tonegawa, Bidirectional switch of the valence associated with a hippocampal contextual memory engram. *Nature* **513**, 426–430 (2014).

14. J. F. Bergan, Y. Ben-Shaul, C. Dulac, Sex-specific processing of social cues in the medial amygdala. *Elife* **3**, e02743 (2014).

15. Y. Li, A. Mathis, B. F. Grewe, J. A. Osterhout, B. Ahanonu, M. J. Schnitzer, V. N. Murthy, C. Dulac, Neuronal Representation of Social Information in the Medial Amygdala of Awake Behaving Mice. *Cell* **171**, 1176-1190.e17 (2017).

16. T. Yamaguchi, D. Wei, S. C. Song, B. Lim, N. X. Tritsch, D. Lin, Posterior amygdala regulates sexual and aggressive behaviors in male mice. *Nat. Neurosci.* **23**, 1111–1124 (2020).

17. X. Zha, L. Wang, Z.-L. Jiao, R.-R. Yang, C. Xu, X.-H. Xu, VMHvl-Projecting Vglut1+ Neurons in the Posterior Amygdala Gate Territorial Aggression. *Cell Rep.* **31**, 107517 (2020).

18. J. N. Ferguson, J. M. Aldag, T. R. Insel, L. J. Young, Oxytocin in the medial amygdala is essential for social recognition in the mouse. *J. Neurosci.* **21**, 8278–8285 (2001).

19. S. Yao, J. Bergan, A. Lanjuin, C. Dulac, Oxytocin signaling in the medial amygdala is required for sex discrimination of social cues. *Elife* **6** (2017).

20. E. L. Stevenson, H. K. Caldwell, Lesions to the CA2 region of the hippocampus impair social memory in mice. *Eur. J. Neurosci.* **40**, 3294–3301 (2014).

21. A. S. Smith, S. K. Williams Avram, A. Cymerblit-Sabba, J. Song, W. S. Young, Targeted activation of the hippocampal CA2 area strongly enhances social memory. *Mol. Psychiatry* **21**, 1137–1144 (2016).

22. K. Kohara, M. Pignatelli, A. J. Rivest, H.-Y. Jung, T. Kitamura, J. Suh, D. Frank, K. Kajikawa, N. Mise, Y. Obata, I. R. Wickersham, S. Tonegawa, Cell type-specific genetic and optogenetic tools reveal hippocampal CA2 circuits. *Nat. Neurosci.* **17**, 269–279 (2014).

23. M. Luo, M. S. Fee, L. C. Katz, Encoding pheromonal signals in the accessory olfactory bulb of behaving mice. *Science* **299**, 1196–1201 (2003).

24. J. He, L. Ma, S. Kim, J. Nakai, C. R. Yu, Encoding gender and individual information in the mouse vomeronasal organ. *Science* **320**, 535–538 (2008).

25. R. Remedios, A. Kennedy, M. Zelikowsky, B. F. Grewe, M. J. Schnitzer, D. J. Anderson, Social behaviour shapes hypothalamic neural ensemble representations of conspecific sex. *Nature* **550**, 388–392 (2017).

26. D. R. Levy, T. Tamir, M. Kaufman, A. Parabucki, A. Weissbrod, E. Schneidman, O. Yizhar, Dynamics of social representation in the mouse prefrontal cortex. *Nat. Neurosci.* **22**, 2013–2022 (2019).

27. L. Kingsbury, S. Huang, T. Raam, L. S. Ye, D. Wei, R. K. Hu, L. Ye, W. Hong, Cortical Representations of Conspecific Sex Shape Social Behavior. *Neuron* **107**, 941-953.e7 (2020).

28. Z. Huang, M. Chung, K. Tao, A. Watarai, M.-Y. Wang, H. Ito, T. Okuyama, Ventromedial prefrontal neurons represent self-states shaped by vicarious fear in male mice. *Nat. Commun.* **14**, 3458 (2023).

29. S. Kira, H. Safaai, A. S. Morcos, S. Panzeri, C. D. Harvey, A distributed and efficient population code of mixed selectivity neurons for flexible navigation decisions. *Nat. Commun.* **14**, 2121 (2023).

30. R. Q. Quiroga, L. Reddy, G. Kreiman, C. Koch, I. Fried, Invariant visual representation by single neurons in the human brain. *Nature* **435**, 1102–1107 (2005).

31. T. J. Tyree, M. Metke, C. T. Miller, Cross-modal representation of identity in the primate hippocampus. *Science* **382**, 417–423 (2023).

32. A. Montagrin, C. Saiote, D. Schiller, The social hippocampus. *Hippocampus* **28**, 672–679 (2018).

33. A. Finkelstein, N. Ulanovsky, M. Tsodyks, J. Aljadeff, Optimal dynamic coding by mixed-dimensionality neurons in the head-direction system of bats. *Nat. Commun.* **9**, 3590 (2018).

34. W. J. Johnston, S. E. Palmer, D. J. Freedman, Nonlinear mixed selectivity supports reliable neural computation. *PLoS Comput. Biol.* **16**, e1007544 (2020).

35. J. O'Keefe, M. L. Recce, Phase relationship between hippocampal place units and the EEG theta rhythm. *Hippocampus* **3**, 317–330 (1993).

36. W. E. Skaggs, B. L. McNaughton, M. A. Wilson, C. A. Barnes, Theta phase precession in hippocampal neuronal populations and the compression of temporal sequences. *Hippocampus* **6**, 149–172 (1996).

37. G. Dragoi, G. Buzsáki, Temporal encoding of place sequences by hippocampal cell assemblies. *Neuron* **50**, 145–157 (2006).

38. D. J. Foster, M. A. Wilson, Hippocampal theta sequences. *Hippocampus* **17**, 1093–1099 (2007).

39. S. Terada, Y. Sakurai, H. Nakahara, S. Fujisawa, Temporal and Rate Coding for Discrete Event Sequences in the Hippocampus. *Neuron* **94**, 1248-1262.e4 (2017).

40. A. Shimbo, E.-I. Izawa, S. Fujisawa, Scalable representation of time in the hippocampus. *Sci Adv* **7** (2021).

41. B. Lasztóczi, T. Klausberger, Hippocampal Place Cells Couple to Three Different Gamma Oscillations during Place Field Traversal. *Neuron* **91**, 34–40 (2016).

42. A. Fernández-Ruiz, A. Oliva, G. A. Nagy, A. P. Maurer, A. Berényi, G. Buzsáki, Entorhinal-CA3 Dual-Input Control of Spike Timing in the Hippocampus by Theta-Gamma Coupling. *Neuron* **93**, 1213-1226.e5 (2017).

43. F. Sharif, B. Tayebi, G. Buzsáki, S. Royer, A. Fernandez-Ruiz, Subcircuits of Deep and Superficial CA1 Place Cells Support Efficient Spatial Coding across Heterogeneous Environments. *Neuron*, doi: 10.1016/j.neuron.2020.10.034 (2020).

44. R. K. Hu, Y. Zuo, T. Ly, J. Wang, P. Meera, Y. E. Wu, W. Hong, An amygdala-to-hypothalamus circuit for social reward. *Nat. Neurosci.* **24**, 831–842 (2021).

45. S. Bariselli, H. Hörnberg, C. Prévost-Solié, S. Musardo, L. Hatstatt-Burklé, P. Scheiffele, C. Bellone, Role of VTA dopamine neurons and neuroligin 3 in sociability traits related to nonfamiliar conspecific interaction. *Nat. Commun.* **9**, 3173 (2018).

46. A. R. Caffé, F. W. van Leeuwen, P. G. Luiten, Vasopressin cells in the medial amygdala of the rat project to the lateral septum and ventral hippocampus. *J. Comp. Neurol.* **261**, 237–252 (1987).

47. N. S. Canteras, R. B. Simerly, L. W. Swanson, Organization of projections from the medial nucleus of the amygdala: a PHAL study in the rat. *J. Comp. Neurol.* **360**, 213–245 (1995).

48. C. Poo, G. Agarwal, N. Bonacchi, Z. F. Mainen, Spatial maps in piriform cortex during olfactory navigation. *Nature* **601**, 595–599 (2022).

49. H. Gelbard-Sagiv, R. Mukamel, M. Harel, R. Malach, I. Fried, Internally generated reactivation of single neurons in human hippocampus during free recall. *Science* **322**, 96–101 (2008).

50. A. Watarai, K. Tao, T. Okuyama, Sexual representation of social memory in the ventral CA1 neurons [Dataset]. *Dryad* (2024); https://doi.org/10.5061/dryad.280gb5mxn.

Acknowledgments: We thank T. Kitanishi and S. Fujisawa for their helpful comments aiding manuscript revision and all the members of the Laboratory for Behavioral Neuroscience (Okuyama Lab) for their advice and assistance.

Funding: This work was supported by JST FOREST Program JPMJFR2143, JST JPMJCR23B1; JSPS KAKENHI Grant Numbers JP18H02544, JP20K21459, JP21H02593, JP22H05140, AMED Grant Number JP21wm0525018, The Naito Foundation, and SECOM Science and Technology Foundation (TO); JSPS KAKENHI Grant Numbers JP20J01468, and JP23K19395 (AW); JSPS KAKENHI Grant Numbers JP19K06951, and JP22K06481 (KT).

Author contributions: Conceptualization: AW, KT, TO; Methodology: AW, KT, TO; Investigation: AW, KT; Visualization: KT; Funding acquisition: AW, KT, TO; Supervision: TO; Writing – original draft: KT, TO; Writing – review & editing: AW, KT, TO

Competing interests: The authors declare that they have no competing interests.

Data and materials availability: All data are available in the main text and supplementary materials or have been deposited to Dryad (*50*).

Supplementary Materials

Materials and Methods

Supplementary Text

Figs. S1 to S9

References (*1–50*)

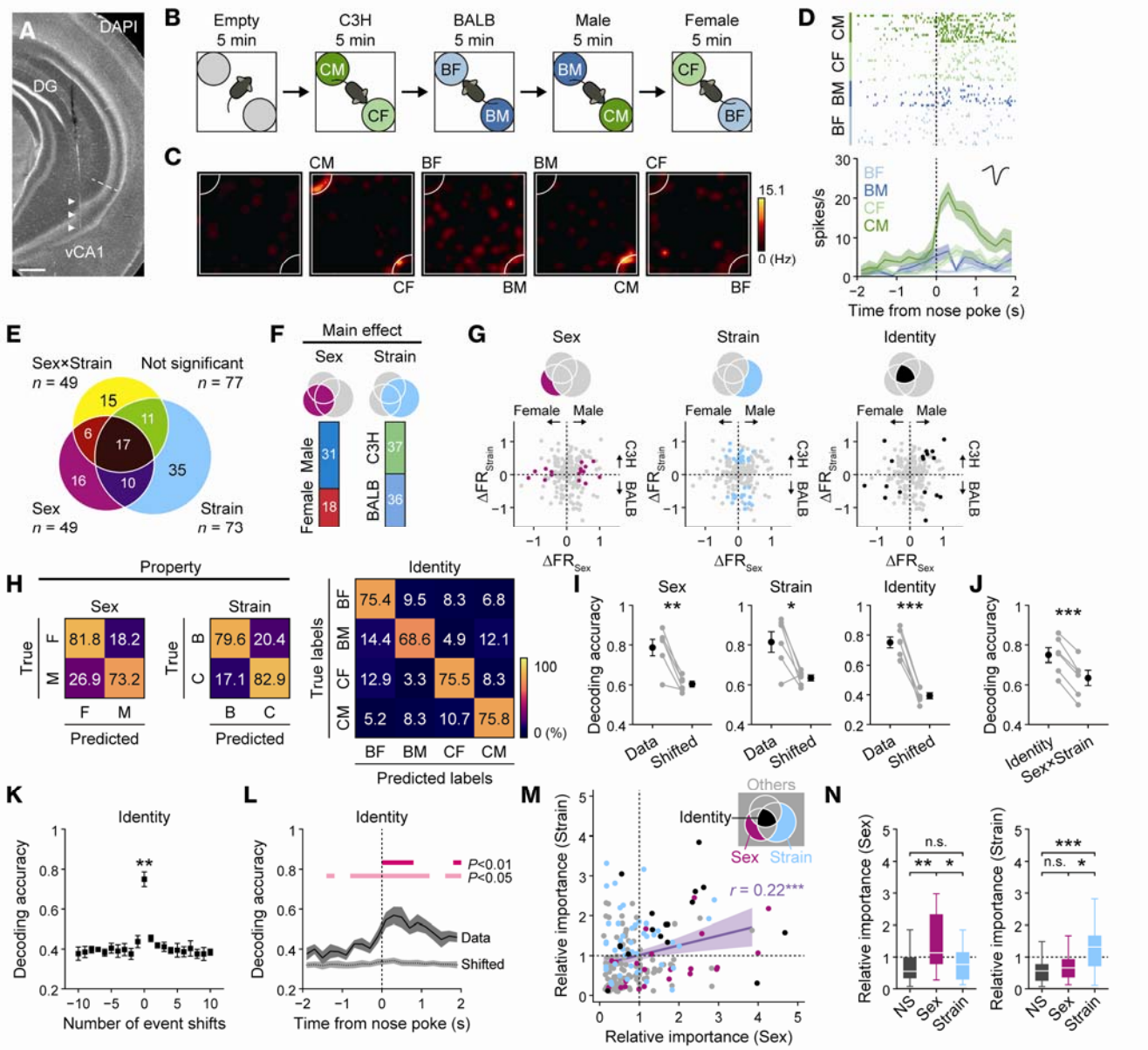

Fig. 1. Ventral CA1 neurons encode the identity and properties of social memory. (**A**) Recording site. Scale bar, 200 µm. (**B**) Paradigm for the four-mouse social interaction test. BF, BM, CF, and CM denote BALB female, BALB male, C3H female, and C3H male mice, respectively. (**C**) Firing-rate heatmaps of a representative CM neuron. (**D**) Peri-event time histogram and raster plots aligned to nose-poke onset for the same neuron as in (C). (**E**) The Venn diagram illustrates the result of a two-way ANOVA for all recorded putative pyramidal cells (n = 187). Significance was determined at $P<0.05$. (**F**) Target preference of sex and strain cells. (**G**) Distribution of sex (n = 16), strain (n = 35), and identity (n = 17) cells on a 2-D map showing differences in z-scored firing rate by the sex and strain of social stimuli. (**H**) Confusion

matrices for decoding sex (left), strain (center), and social identity (right), averaged over the subjects (n = 6 mice). The matrices were normalized by each row to represent true-positive and false-negative rates. (**I**) Decoding accuracy of classifiers constructed with real or shifted event labels. *P<0.05, **P<0.01, ***P<0.001, paired t-test. (**J**) Comparison of decoding accuracy of identity classifiers with the linear combination of decoding accuracy of sex classifiers and strain classifiers. ***P<0.001, paired t-test. (**K**) Decoding the accuracy of the classifier with real data (shifts = 0) and event-shifted labels (shifts = ±10 events) for identity. **P<0.01 for shifts = 0 vs. ±1, Tukey–Kramer multiple comparisons. (**L**) Decoding the accuracy for identity across time (mean ± SEM, n = 6 mice). Significance was assessed by Tukey–Kramer multiple comparisons. (**M**) Scatterplot of the relative importance of sex decoding versus strain decoding and its correlation (r = 0.22, P<0.002, permutation test) for all recorded pyramidal cells (n = 187). Red dots represent sex cells (n = 16), blue dots represent strain cells (n = 35), black dots represent social identity cells (n = 17), and gray dots indicate all other pyramidal cells (n = 136). (**N**) Comparison of relative importance between sex cells and strain cells. *P<0.05, **P<0.01, ***P<0.001, Wilcoxon rank-sum test.

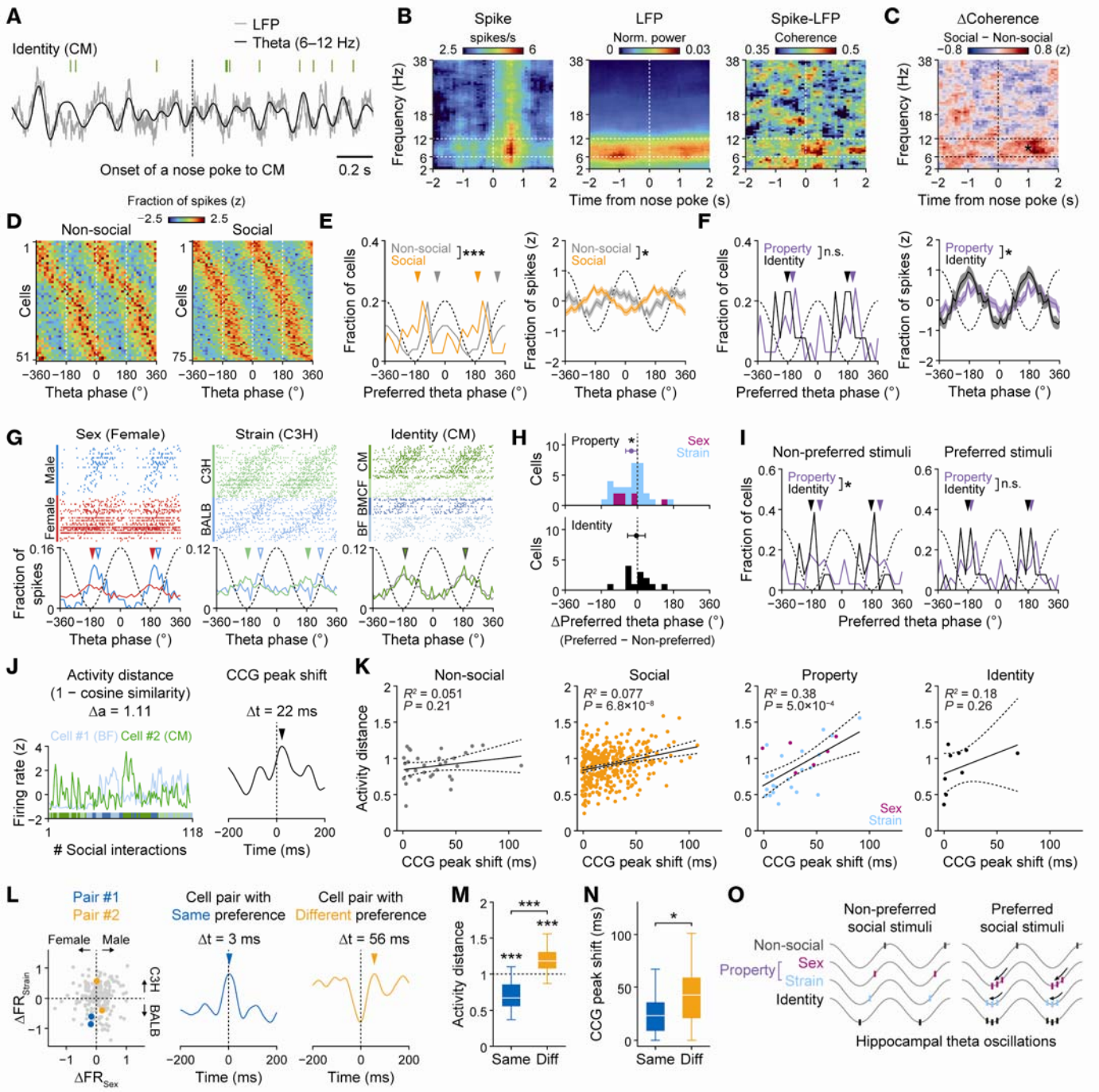

Fig. 2. Theta phase-specific encoding of social identity and its properties. (**A**) LFP trace and spike timings for a representative neuron around the onset of social interaction, with spike timings marked by green vertical lines. (**B**) Spike spectrogram (left) and spike-LFP coherogram (right) for the neuron in (A) around the onset of social interaction. Note the absence of an increase in instantaneous theta power during the interaction (center). (**C**) Comparison of average spike-LFP coherograms between social cells and non-social cells. *P<0.05, permutation test. (**D**)

Spike theta phase distributions for non-social cells (n = 51) and social cells (n = 75), organized by preferred phases. Only cells with significant theta modulation (P<0.01, Rayleigh test) were considered. (**E**) Left, distribution of preferred theta phases for social cells and non-social cells. ***P<0.001, Watson–Williams test. Right, mean z-scored proportions of spike theta phases for social cells and non-social cells. *P<0.05, permutation test. (**F**) Analysis similar to (E) but for comparisons between social property cells and social identity cells. *P<0.05, permutation test. (**G**) Raster plot and spike theta phase distribution from left to right for example sex cell (female preferred), strain cell (C3H preferred), and identity cell (CM preferred). Spike raster rows for each social interaction were organized by the preferred theta phases of that trial. Mean theta phases of spikes for preferred and non-preferred social stimuli are represented by filled and empty triangles, respectively. (**H**) Distribution of preferred spike phase differences when interacting with preferred versus non-preferred social stimuli. *P<0.05, one-sample test for the mean angle. Error bars represent 95% confidence intervals. (**I**) Distribution of preferred theta phases for social property cells and social identity cells under interacting with preferred or non-preferred social stimuli. *P<0.05, Watson–Williams test. (**J**) Left, response series to social stimuli across trials for two example social identity cells recorded simultaneously, with cell #1 preferring BF and cell #2 preferring CM. The color code at the bottom indicates the social stimulus target in each interaction. Right, spike cross-correlogram (CCG) for the same cell pair, shown in arbitrary units. (**K**) Correlation between the temporal shift in CCG peaks and the pairwise distance in neuronal activity during social interactions for pairs of non-social (n = 33), social (n = 365), sex and strain (n = 28), and identity (n = 9) cell pairs. (**L**) Representation of two cell pairs on a 2-D map showing differences in z-scored firing rate by sex and strain of social stimuli. (**M**) Comparison of pairwise distances in social neuronal activity between cell pairs with the same (n = 44) versus different (n = 21) social property preferences. ***P<0.001, Wilcoxon rank-sum test. (**N**) Comparison of CCG peak shifts between cell pairs with the same versus different social property preferences. *P<0.05, Wilcoxon rank-sum test. (**O**) Schema summarizing a rate and temporal coding strategy in vCA1 for representing social identity and properties.

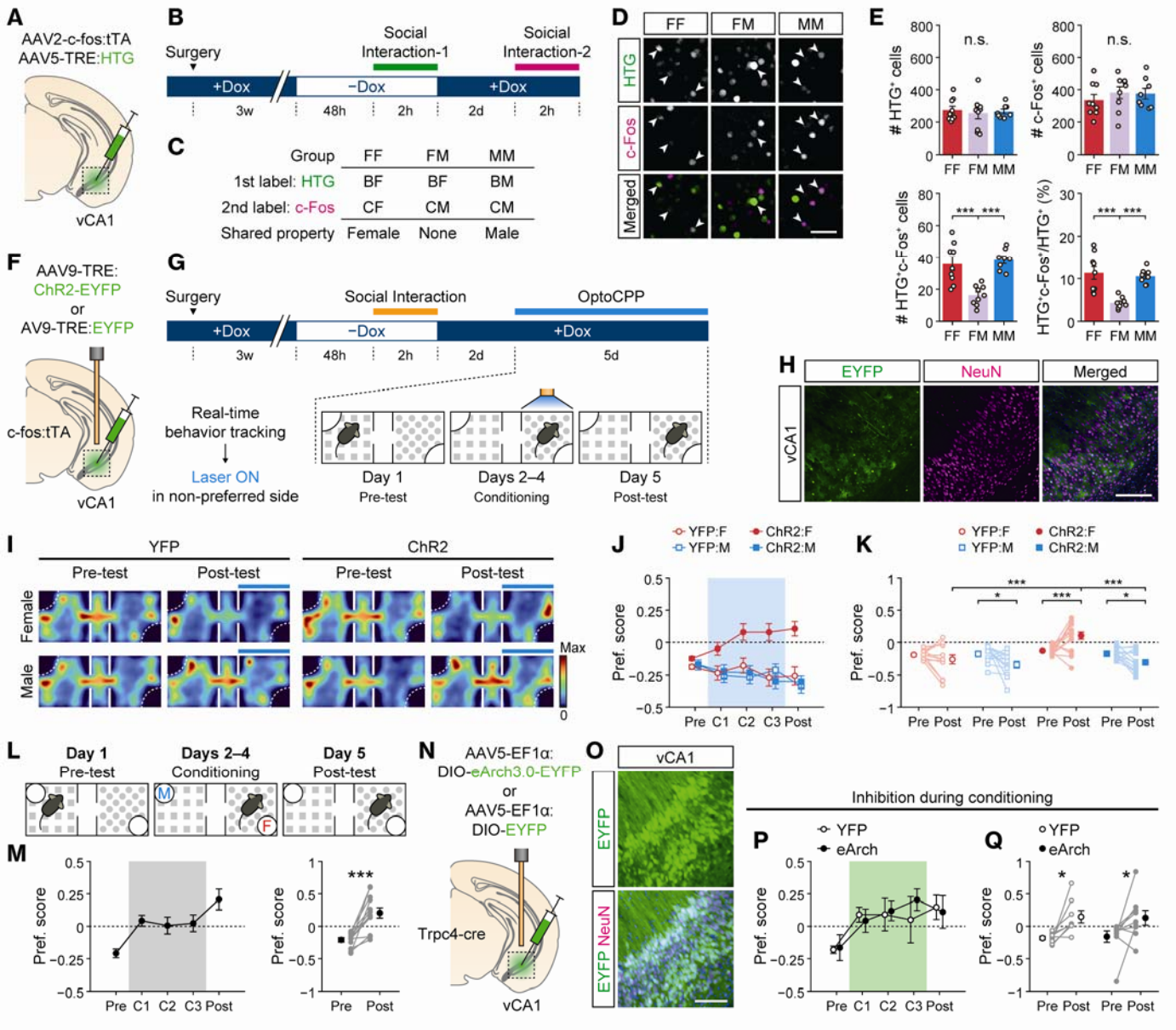

Fig. 3. Reactivation of female social memory in vCA1 exerts positive valence. (**A**) Schematic representation of virus-mediated tTA/TRE system targeting vCA1 to label social interaction-activated neurons. (**B**) Experimental protocol for dual labeling of activated neurons. Neurons activated by the first social interaction were labeled by HTG expression, whereas those activated by the second interaction were detected by c-Fos expression. (**C**) Labeling paradigm for the three behavioral groups. (**D**) Representative images of labeled vCA1 neurons. Scale bar, 50 µm. (**E**) Number of HTG$^+$ cells, number of c-Fos$^+$ cells, number of HTG$^+$c-Fos$^+$ double-positive cells, and ratio of double-positive cells to HTG$^+$ cells. ***P<0.001, Tukey–Kramer multiple comparisons. (**F**, **G**) Schematic (F) and experimental protocol (G) for optogenetic conditioned

place preference (optoCPP) test targeting vCA1. (**H**) Representative image of vCA1 showing EYFP expression. Scale bar, 100 µm. (**I**) Occupancy maps averaged across subjects before (Pre-test) and after (Post-test) the optogenetic conditioning. Filled blue bars indicate the stimulated side during conditioning (i.e., non-preferred side during Pre-test). (**J**) Temporal development of the preference score over conditioning (n = 12–16 mice for each group). (**K**) Comparison of the preference score between Pre-test and Post-test. *P<0.05, ***P<0.001, Tukey–Kramer multiple comparisons. (**L**) Experimental protocol for conditioned place preference test with real social stimuli. (**M**) Left: temporal development of the preference score over conditioning (n = 12 mice). Right: comparison of the preference score between Pre-test and Post-test. ***P<0.001, paired t test. (**N**) Schematic of optogenetic inhibition targeting vCA1. (**O**) Representative image of virus expression. Scale bar, 100 µm. (**P**, **Q**) Temporal development (P) and comparison between Pre-test and Post-test (Q) of the preference score. n = 8 (YFP) and 9 (eArch) mice. *P<0.05, Tukey–Kramer multiple comparisons.

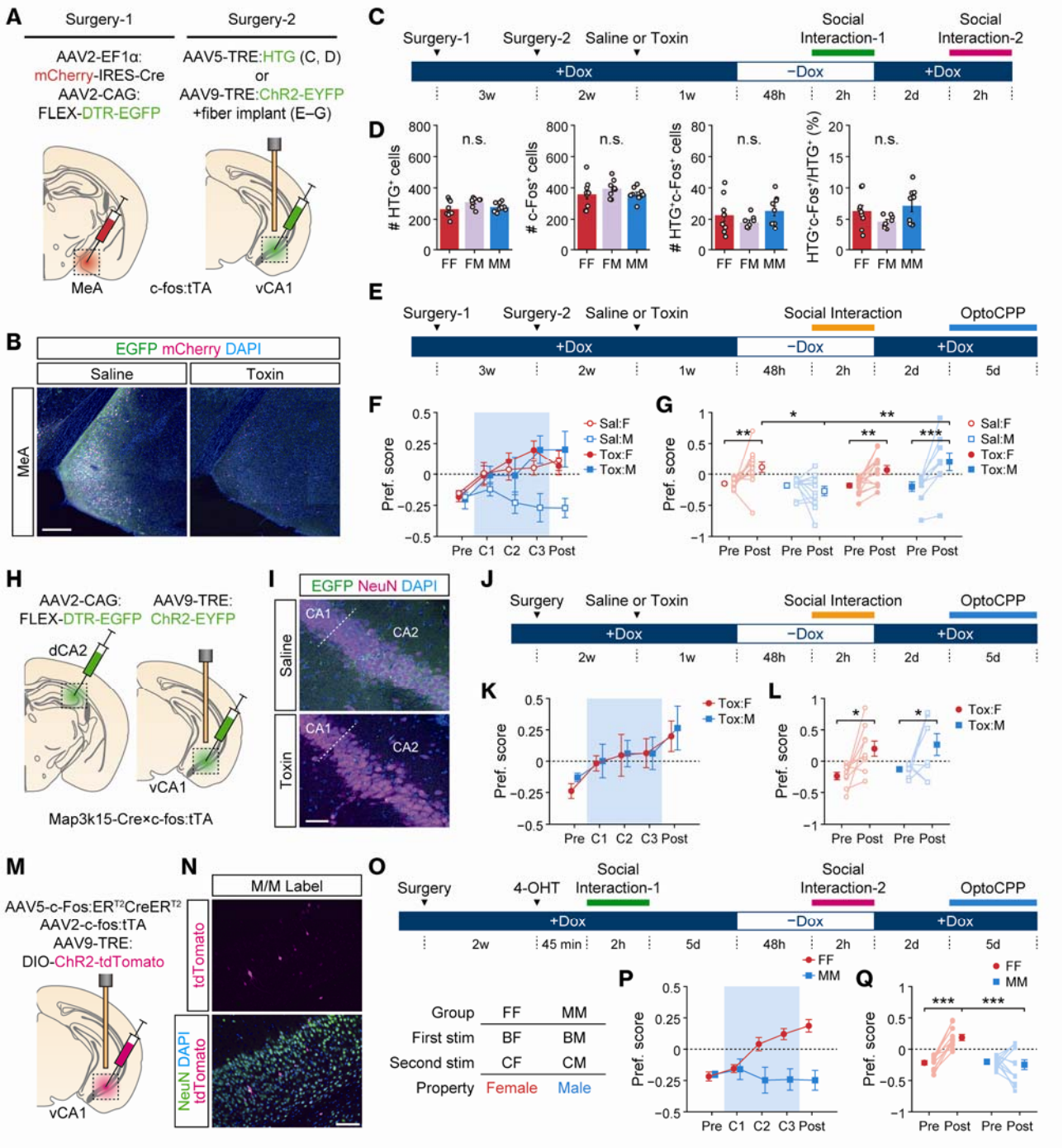

Fig. 4. MeA ablation, dCA2 ablation, and FF/MM. (**A**) Schematic of MeA ablation using Cre-inducible diphtheria toxin receptor (DTR) and activity-dependent cell labeling. (**B**) Representative image of MeA. Scale bar, 200 µm. (**C**) Experimental protocol for dual labeling of activated neurons after MeA ablation. (**D**) Left to right: number of HTG$^+$ cells, number of c-Fos$^+$ cells, number of HTG$^+$c-Fos$^+$ double-positive cells, and the ratio of double-positive cells to HTG$^+$ cells. (**E**) Experimental protocol for optoCPP test following MeA ablation. (**F**) Temporal

development of the preference score over conditioning (n = 9–13 mice for each group). (**G**) Comparison of the preference score between Pre-test and Post-test. *P<0.05, **P<0.01, ***P<0.001, Tukey–Kramer multiple comparisons. (**H**) Schematics of dCA2 ablation using Cre-inducible DTR and activity-dependent cell labeling targeting. (**I**) Representative images of dCA2. Scale bar, 100 µm. (**J**) Experimental protocol for optoCPP test following dCA2 ablation. (**K**) Temporal development of the preference score over conditioning (n = 8–9 mice for each group). (**L**) Comparison of the preference score between Pre-test and Post-test. *P<0.05, Tukey–Kramer multiple comparisons. (**M**) Schematics of intersectional labeling using Cre-inducible DTR and activity-dependent cell labeling targeting. (**N**) Representative images of vCA1. Scale bar, 100 µm. (**O**) Experimental protocol for optoCPP test. (**P**) Temporal development of the preference score over conditioning (n = 11–13 mice for each group). (**Q**) Comparison of the preference score between Pre-test and Post-test. ***P<0.001, Tukey–Kramer multiple comparisons.